

# A 300-GHz Transmitter Front End With $-4.1$ -dBm Peak Output Power for Sub-THz Communication Using 130-nm SiGe BiCMOS Technology

Jiayang Yu, *Student Member, IEEE*, Jixin Chen<sup>ID</sup>, *Member, IEEE*, Peigen Zhou<sup>ID</sup>, *Member, IEEE*,  
Zekun Li<sup>ID</sup>, *Graduate Student Member, IEEE*, Huanbo Li, Pinpin Yan, *Member, IEEE*,  
Debin Hou<sup>ID</sup>, *Member, IEEE*, and Wei Hong<sup>ID</sup>, *Fellow, IEEE*

**Abstract**—This article presents a compact 300-GHz transmitter front end manufactured in a 130-nm SiGe BiCMOS process. The transmitter consists of a 240-GHz amplifier multiplier chain (AMC) and a modified 300-GHz Gilbert mixer. Limited by the space between top two thick metal layers of the SiGe process, the coupling coefficient between the coils, which form a transformer-based balun, is usually small at subterahertz (THz). Therefore, the vertical or horizontal coupling single-turn transformer-based balun will exhibit large insertion loss at around 300 GHz. In this work, a self-shielded Marchand balun (SSMB) with an enhancement to the coupling coefficient is proposed, which is realized by a novel multilayer metal topology with self-shielded coupling (SSC). The AMC is composed of a 120-GHz frequency doubler, a 120-GHz two-stage power amplifier (PA), and a two-way power synthesis balanced frequency doubler. This AMC exhibits a measured peak output power of 5.5 dBm at 252 GHz, with 48-GHz 3-dB bandwidth from 212 to 260 GHz. The transmitter chip achieves a maximum output power of  $-4.1$  dBm at 300 GHz and delivers an output power better than  $-10$  dBm from 270 to 315 GHz. Over the 30-GHz 3-dB bandwidth from 280 to 310 GHz, the transmitter shows a maximum  $OP_{1dB}$  of  $-6.5$  dBm at 296 GHz, a peak conversion gain of  $-11.2$  dB at 298 GHz, and a local oscillator (LO)-to-RF leakage rejection better than 40 dB, with only 300-mW dc power consumption. Compared with other state of the arts, the transmitter exhibits a comparable output power among silicon-based transmitters near 300 GHz.

**Index Terms**—Amplifier multiplier chain (AMC), power combining, self-shielded Marchand balun (SSMB), subterahertz (THz) transmitter, 300 GHz.

## I. INTRODUCTION

AS WIRELESS technology advances, wireless communication is facing a new data rate challenge in the level of terabytes. Compared to microwave and millimeter-wave (mm-wave) communication, terahertz (THz) communication

has a larger transmission bandwidth and transmission rate because of a higher carrier frequency and richer spectrum resources. Besides, the IEEE 802.15.3d standard reported in October 2017 defines 32 2.16-GHz-wide channels between 252 and 325 GHz (300-GHz band) for up to 100-Gb/s data rate [1]. III–V group compound semiconductor technology has traditionally been adopted for THz communication, but recent advances in silicon-based technologies have resulted in SiGe heterojunction bipolar transistors (HBTs) with cutoff frequency  $f_T$  approaching 300 GHz [2]. This has made silicon-based process a good low-cost alternative for III–V semiconductors [3], [4]. However, due to the limited maximum oscillation frequency ( $f_{max}$ ) of transistors and low efficiency of passive components, the generation of a milliwatt-level local oscillator (LO) signal based on existing silicon processes for sub-THz communication system [5] remains a challenge. Studies on silicon-based amplifiers at frequencies above 200 GHz have shown remarkable advancement in the past few years [6]–[11]. At present, the reported maximum output power of sub-THz silicon-based power amplifier (PA) is 13.5 dBm at 240 GHz (above 200 GHz) [11]. However, it is still a challenge to deliver milliwatt-level output power using silicon-based processes at the 300-GHz band.

At sub-THz, the RF ground plane would introduce seriously parasitic inductance, which will deteriorate the stability of the transmitter. Besides, the connection of bypass decoupling capacitors would introduce extra parasitic signal paths to the ground, which will decrease the power-handling capability besides stability issues. Thus, the differential topology is usually adopted for sub-THz circuit design to take advantage of the virtual ground [11], [12]. For sub-THz differential circuits, the single-ended-to-differential conversion is an extremely critical component due to the limited active gain. In the microwave and mm-wave bands, the integrated single-turn transformer-based balun is a compact and low-loss solution. However, at the sub-THz band, the size of the transformer is relatively small, which will lead to self-resonance and large insertion loss.

The topology of transmitters at sub-THz frequency band can be broadly divided into two categories, which are directly mixing structure and subharmonic mixing architecture.

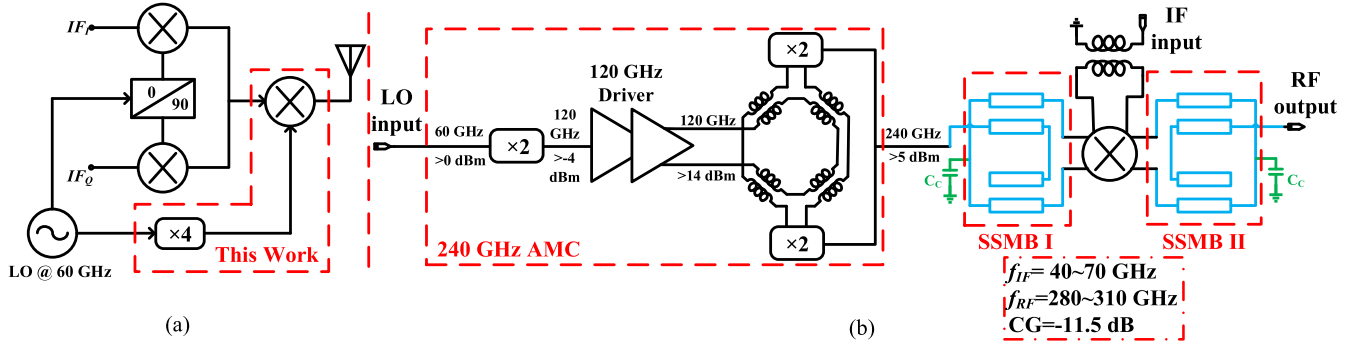
Manuscript received February 25, 2021; revised May 20, 2021; accepted July 16, 2021. Date of publication August 20, 2021; date of current version November 4, 2021. This work was supported in part by the National Natural Science Foundation of China under Grant 61941103. (Corresponding authors: Jixin Chen; Peigen Zhou.)

The authors are with the State Key Laboratory of Millimeter Waves, Southeast University, Nanjing 210096, China (e-mail: jxchen@seu.edu.cn; pgzhou@seu.edu.cn).

Color versions of one or more figures in this article are available at <https://doi.org/10.1109/TMTT.2021.3103574>.

Digital Object Identifier 10.1109/TMTT.2021.3103574

0018-9480 © 2021 IEEE. Personal use is permitted, but republication/redistribution requires IEEE permission.  
See <https://www.ieee.org/publications/rights/index.html> for more information.



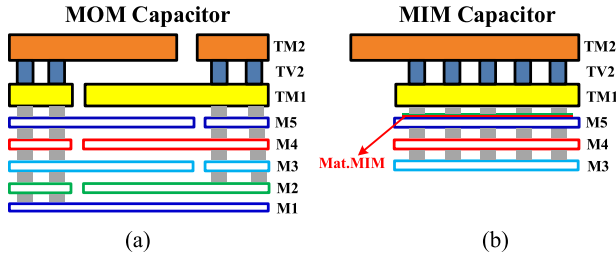
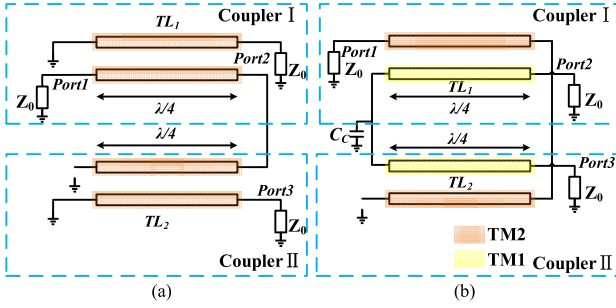


Fig. 2. Layout of (a) MOM capacitor and (b) MIM capacitor.

Fig. 3. Equivalent schematic of (a) ideal Marchand balun and (b) modified Marchand balun with  $C_C$ .

the IF ( $f_{IF}$ ) is from 40 to 70 GHz, and the output sub-THz signal's frequency range is from 280 to 310 GHz ( $f_{RF}$ ). The  $\times 4$  multiplier chain consists of a 120-GHz doubler, a 120-GHz driver, and a 240-GHz doubler. To enhance LO driving power, the output stage of the LO chain adopts a power-combining structure with two doubler cells. The two-stage 120-GHz gain-boosting driver can supply sufficient output power to drive the 240-GHz doubler. The upconversion mixer is based on the Gilbert cell, but the differential pair at the IF input end is abandoned and replaced by a transformer-based balun. The LO input termination and RF output termination are both matched with the proposed self-shielded Marchand balun (SSMB).

#### IV. ANALYSIS OF THE SSMB

##### A. Marchand Balun Analysis

Transformer-based baluns are widely used for single-ended-to-differential conversion due to its capability of achieving impedance matching with moderate chip size. However, the dimension of the balun decreases rapidly as the targeted frequency increases, which makes the fabrication extremely difficult. Meanwhile, the decreasing mutual coupling factor of the transformer will increase its insertion loss at the sub-THz frequency band. Fortunately, the Marchand balun is a better substitute at the sub-THz band. Several works have been proposed to realize the Marchand balun at mm-wave and sub-THz band [29]–[32].

For an ideal model of a compact backward-wave coupler, the electrical length of the coupled line is  $\lambda/4$ , and the scattering matrix of the four-port couplers with infinite directivity and coupling factor  $k$  is given by (1) according to [29].

Fig. 3(a) shows the structure of a traditional Marchand balun, which is composed of two cascaded backward-wave couplers. The S matrix of the Marchand balun as shown

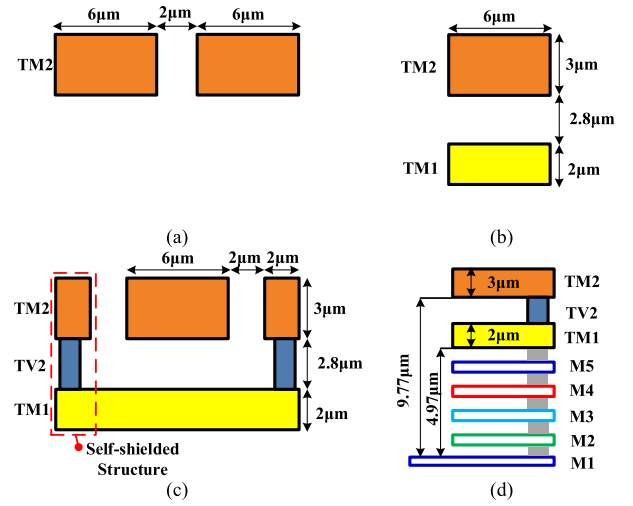


Fig. 4. Cross-sectional of (a) coplaner coupled line, (b) stacked coupled line, (c) proposed stacked coupled line with self-shielded structure, and (d) metal layer of the process.

in Fig. 3(a) can be calculated by considering the S matrix of the two identical backward-wave couplers and can be expressed as follows [29], [30]:

$$[S]_{\text{coupler}} = \begin{bmatrix} 0 & -j\sqrt{1-k^2} & k & 0 \\ -j\sqrt{1-k^2} & 0 & 0 & k \\ k & 0 & 0 & -j\sqrt{1-k^2} \\ 0 & k & -j\sqrt{1-k^2} & 0 \end{bmatrix} \quad (1)$$

$$[S]_M = \begin{bmatrix} \frac{1-3k^2}{1+k^2} & j\frac{2k\sqrt{1-k^2}}{1+k^2} & -j\frac{2k\sqrt{1-k^2}}{1+k^2} \\ j\frac{2k\sqrt{1-k^2}}{1+k^2} & \frac{1-k^2}{1+k^2} & \frac{2k^2}{1+k^2} \\ -j\frac{2k\sqrt{1-k^2}}{1+k^2} & \frac{2k^2}{1+k^2} & \frac{1-k^2}{1+k^2} \end{bmatrix} \quad (2)$$

Due to the multilayer metal characteristics of the silicon-based process, the Marchand balun can also be realized by the vertical coupling of the top two thick metal layers. For the stacked balun made of the top two thick metal layers, the short end of the two couplers in Fig. 3(a) can be connected together and RF-grounded by a capacitor  $C_C$  [see in Fig. 3(b)]. The balance performance of the Marchand balun can be improved by the capacitor  $C_C$ , and the supply voltage can be fed at this common node, which will also result in a compact layout design.

##### B. Coupled Line Analysis

For the Marchand balun, it is important to design a reliable coupling transmission line with high performance. The cross-sectional view of different quarter-wavelength coupled lines is shown in Fig. 4. From the above analysis, a coupling factor of  $-4.8$  dB is required for an ideal Marchand balun composed of  $\lambda/4$  coupled lines. Actually, the required coupling factor

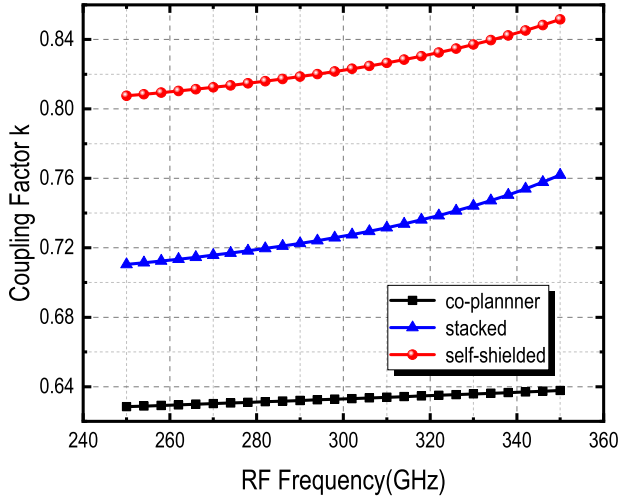


Fig. 5. Simulated coupling factor of the three types of  $\lambda/4$  coupled lines.

is also concerned about load terminations and the electrical length of coupled line. When the balun's load terminations changes from  $Z_0$  to  $Z_L$ , the transmission parameter  $S_{21}$  of an ideal Marchand balun composed of  $\lambda/4$  coupled lines can be changed to [29]

$$S_{21} = S_{31} = j \frac{2k\sqrt{1-k^2}\sqrt{\frac{Z_L}{Z_0}}}{1+k^2\left(2\frac{Z_L}{Z_0}-1\right)}. \quad (3)$$

To achieve optimum power transfer of  $-3$  dB at each port, the needed coupling factor can be estimated by

$$k = \frac{1}{\sqrt{2\frac{Z_L}{Z_0}+1}}. \quad (4)$$

Considering the impedance matching, for example, the differential output impedance at mixer RF port is  $(14.2-j \times 21.67) \Omega$  and the load impedance is  $50 \Omega$ , a coupling factor of 0.86 is required. In Fig. 5, the coupling factor of three types of  $\lambda/4$  coupled lines is compared. According to the simulation results, the proposed self-shielded coupled line (SSCL) shows a better coupling factor. For the coplanar coupled line, the low coupling factor of 0.62 will cause 3-dB extra insertion loss without other matching networks.

Apart from the coupling factor, the transmission mode of the coupled line should be concerned. The scattering matrix in (1) is based on a TEM-type backward-wave coupler. Considering a quasi-TEM type coupler such as a microstrip line-based coupler, the phase velocities of even and odd modes are unequal ( $\beta_e \neq \beta_o$ ). Also, some of the electronic field components will occur in the propagation direction, which means that transmission power leaks into medium. An effective solution to compensate for this difference is to design coupled line with different widths.

In this work, the SSCL is proposed, as shown in Fig. 4(c). This self-shielded structure makes broadside coupling and edge coupling existing at the same time compared with other coupled lines, which increases the total coupling factor dramatically, as shown in Fig. 5. Finally, the proposed SSCL

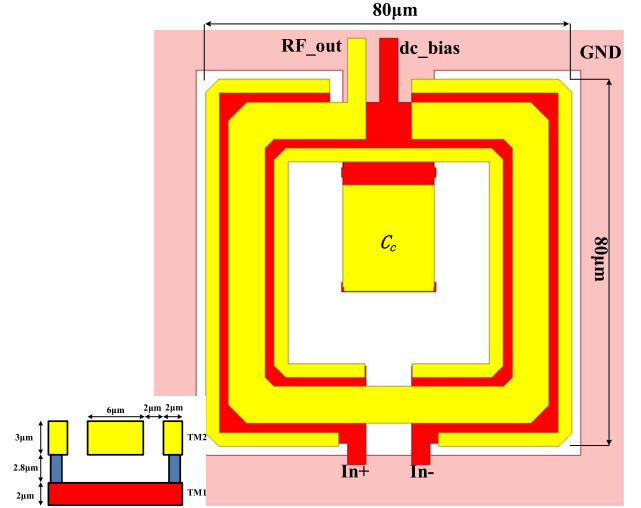


Fig. 6. Layout top view of the proposed SSMB II at RF port of the mixer.

achieves a coupling factor of over 0.8 and makes the low output impedance easily matched to the  $50\text{-}\Omega$  load. Besides, the proposed structure also compensates for the difference of phase velocities and degrades the electronic field component in the propagation direction. Compared with the stacked coupled line, the insertion loss is decreased by using the proposed SSC structure.

### C. Self-Shielded Marchand Balun Design

In this design, a compact stacked Marchand balun based on the SSCL is proposed for LO and RF matching in the mixer block. The top view of SSMB II at RF port in the mixer is shown in Fig. 6. The coupling factor of the coupled line is 0.83 and it is close to the demand of output impedance matching  $[(14.2-j \times 21.67) \Omega]$  from the previous analysis.  $\lambda/4$  is about  $125 \mu\text{m}$  at the working frequency in this medium and a balun with a dimension of  $80 \mu\text{m} \times 80 \mu\text{m}$  can well match the output impedance to  $50 \Omega$ . A high-quality-factor MOM capacitor  $C_C$  is introduced at the common node of the secondary coil to improve the phase and amplitude balance performance of the Marchand balun. Also, the dc voltage can be fed through the virtual ground node. To ensure RF grounding, the capacitance should be over  $150 \text{ fF}$ . However, if the capacitance of  $C_C$  is too large, it will take a large area and make the realization of layout difficult. Finally, an optimized  $C_C$  of  $200 \text{ fF}$  is selected, which achieves an amplitude imbalance of less than  $1 \text{ dB}$  and a phase imbalance of less than  $4^\circ$  from  $250$  to  $330 \text{ GHz}$ , as the simulated results shown in Fig. 7. The electromagnetic (EM) simulation results show that the output balun matches the differential output impedance of  $(14.2-j \times 21.67) \Omega$  to the single-end  $50 \Omega$  load with about  $1.5 \text{ dB}$  insertion loss. The input balun SSMB I can be designed in a similar method, of which the insertion loss is about  $1.4 \text{ dB}$ . This is a much better performance compared with the Marchand balun based on coupled lines in Fig. 4(a) and (b). Compared with other matching networks realized by stacked or coplaner balun at  $300 \text{ GHz}$ , the insertion loss is improved by more than  $1.2 \text{ dB}$ , as shown in Fig. 8.



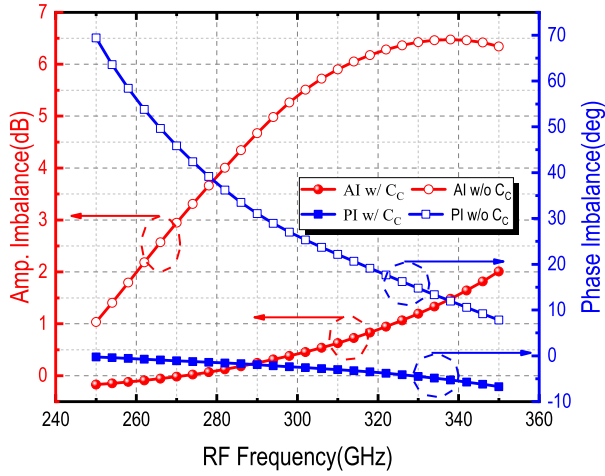


Fig. 7. Amplitude and phase imbalance of the SSMB with and without capacitor  $C_C$ .

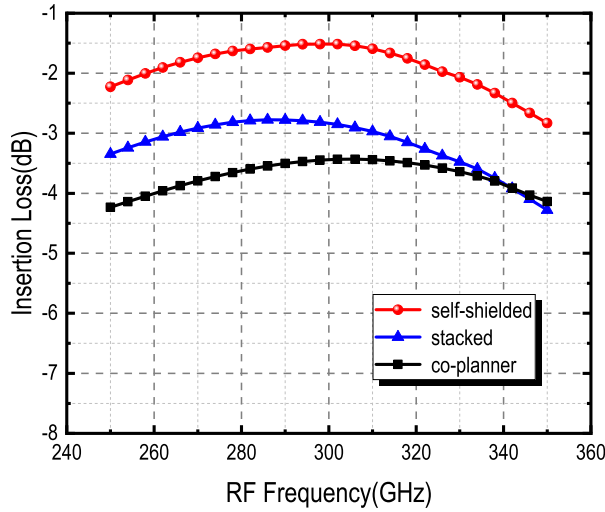


Fig. 8. Simulated insertion loss of Marchand baluns based on three types of coupled lines.

## V. CIRCUIT DESIGN

In this 300-GHz transmitter, the mixer's output power determines the wireless link distance, and LO-to-RF isolation limits the transmitter functionality. Besides, the AMC's driving ability limits the transmitter's conversion gain.

### A. Mixer Design

The schematic of the 300-GHz mixer based on modified Gilbert topology is shown in Fig. 9. Because of insufficient maximum available gain of the active devices and high insertion loss of the passive components, it is a challenge to design a 300-GHz PA with sufficient output power and wide bandwidth. Therefore, the 300-GHz transmitter is designed without a PA at the output. As the operating frequency is close to the transistor's cutoff frequency, the differential pair transistors below the Gilbert core in the traditional structure become lossy and limit the linearity of the mixer. As a result, a modified Gilbert topology without the  $g_m$  stage is adopted,

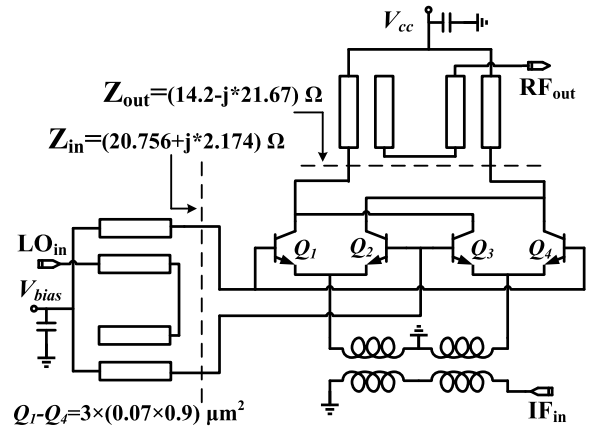


Fig. 9. Schematic of the 300-GHz modified Gilbert mixer.

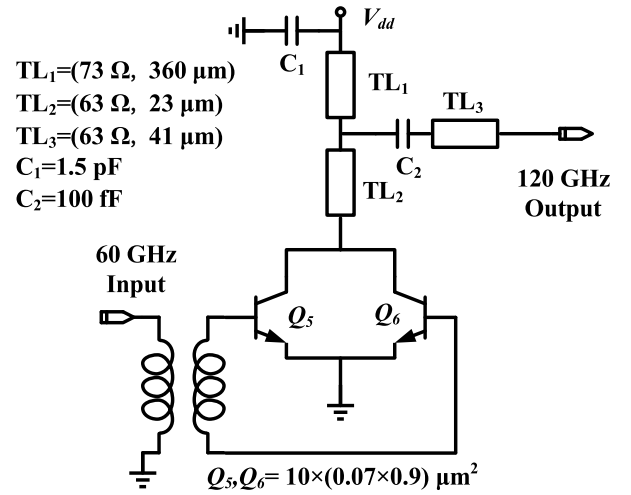


Fig. 10. Schematic of the 120-GHz doubler.

as shown in Fig. 9. In the modified mixer, the  $g_m$  stage is replaced by a transformer-based balun, and the balun also acts as the matching network for the single-ended 60-GHz IF input port. The LO input and RF output network utilize the proposed SSMB for impedance matching, which realizes a single-ended-to-differential conversion with about 1.4- and 1.5-dB insertion loss, respectively. Benefiting from the proposed SSMB, the conversion gain of the mixer has increased by more than 2 dB compared with the matching network realized by the traditional vertical or horizontal coupling Marchand balun.

The size of the transistors ( $Q_1$ – $Q_4$ ) used in the mixing core has been optimized to make a tradeoff between conversion gain and linearity. Transistors of smaller size will obtain higher conversion gain with lower LO-drive power requirement, while it will lead to a lower  $OP_{1dB}$ . To minimize the LO power generation requirements (which is limited by the output power of the AMC), the transistors with the size of  $A_e = 3 \times (0.07 \times 0.9) \mu m^2$  were selected to achieve better output power and also keep the 5-dBm LO input drive power satisfying the requirements for measurement.

The mixer achieves a simulated conversion gain of  $-10.5$  dB at 300 GHz. The saturated output power is simulated



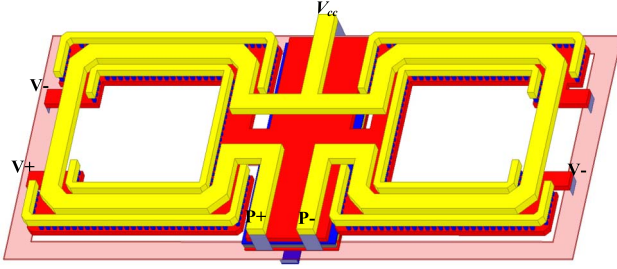


Fig. 13. 3-D model of the transformer-based power splitter.

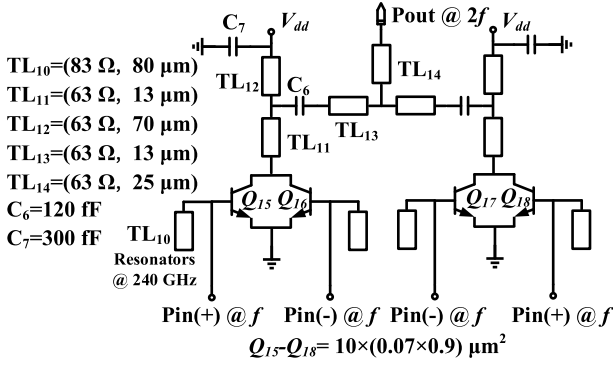


Fig. 14. Schematic of the 240-GHz doubler.

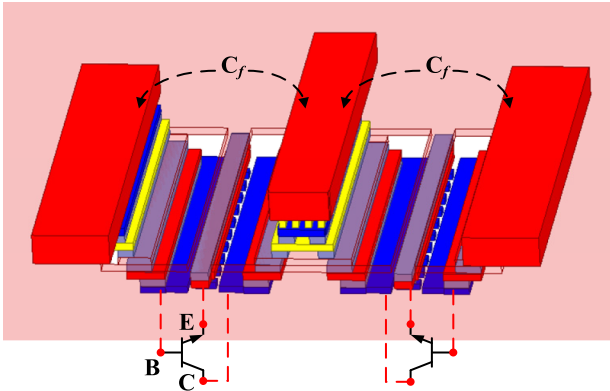


Fig. 15. Proposed optimal transistor layout with stair-like interconnection utilized.

and base bias point. Based on the available fundamental drive power (9 dBm) and harmonic-balance simulation of the doubler, the device size of  $A_e = 10 \times (0.07 \times 0.9)\ \mu\text{m}^2$  is chosen for higher output power with a base bias voltage of 0.6 V and a supply voltage of 1.6 V. The layout of the doubler core is also optimized for better performance at the sub-THz band. The interconnection metal vias are required to connect the top thick metal layer TM2 to the transistor's output interface (metal layer M1). However, two parallel vertical metal vias (M1 to TM2) will suffer from serious coupling at the sub-THz frequency band, which is expressed by a feedback capacitance  $C_f$ , as shown in Fig. 15. The Miller effect caused by  $C_f$  will deteriorate the output power (see in Fig. 15). In this design, a stair-like interconnection [35] is utilized, as shown in Fig. 15. With this method, the coupling capacitance  $C_f$  is

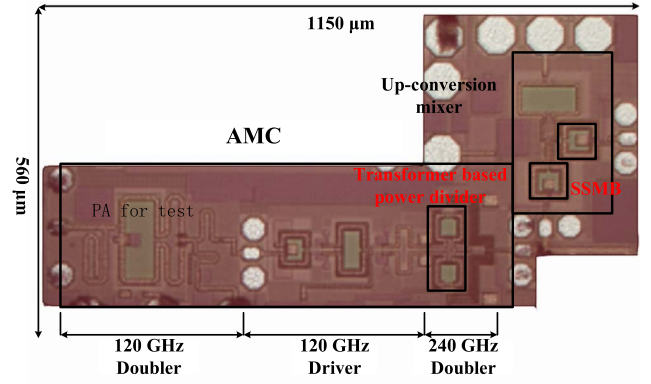


Fig. 16. Die photograph of the proposed transmitter.

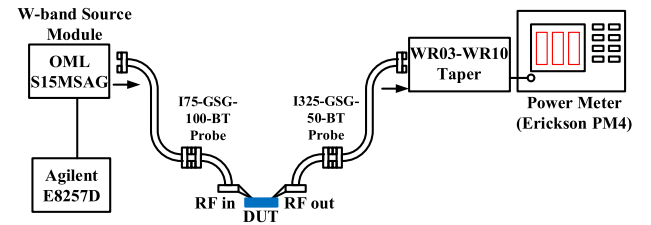


Fig. 17. Measurement setup of the LO chain.

reduced from 13.6 to 8.1 fF at 300 GHz when compared to the traditional straight-up layout.

For a compact layout design, an open stub rather than a short stub is used as the second-harmonic reflector to enhance the second-harmonic's output power. With the  $\lambda/4$  open stub, the output power of the second harmonic drops fast when the working frequency is higher than the frequency point corresponding to the maximum second-harmonic output power [23]. The electrical length of the open stub is optimized to make a tradeoff between peak output power and bandwidth. Through EM simulation, the electrical length of the reflector is set to be  $65^\circ$  in this design. In order to make the layout more compact, lower metal layers M1–M5 are used to implement the reflectors. The output is combined and matched to a 50- $\Omega$  impedance shown in Fig. 14. The output network is composed of transmission lines  $TL_{11}$ ,  $TL_{12}$ ,  $TL_{13}$ , and  $TL_{14}$  and capacitor  $C_6$  enabling a high-pass characteristic for better fundamental frequency suppression. Since the low quality factor of the MIM capacitor will lead to self-resonance at the sub-THz band, the bypass capacitor  $C_7$  adopts an MOM capacitor as an alternative.

The multiplier chain achieves a simulated peak output power of 6.5 dBm at 238- and 55-GHz 3-dB bandwidth from 211 to 266 GHz.

## VI. MEASUREMENT RESULTS

The transmitter system is fabricated in the IHP 130-nm SiGe BiCMOS process. This technology provides seven metal layers for routing, where the top two thick metal layers can be used for the low-loss transmission lines. The die micrograph of the 300-GHz transmitter is shown in Fig. 16. RF pads are inserted

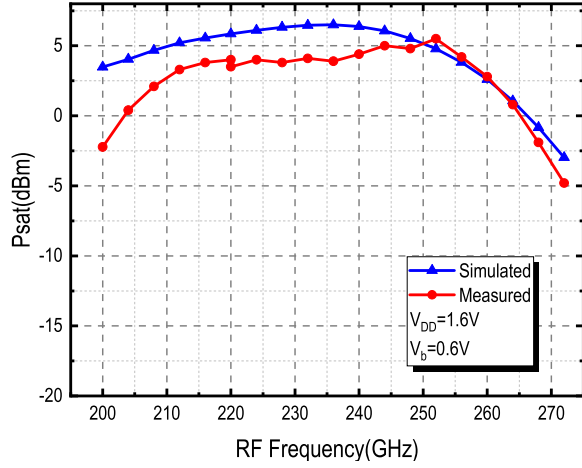


Fig. 18. Simulated and measured output power versus frequency of the multiplier chain.

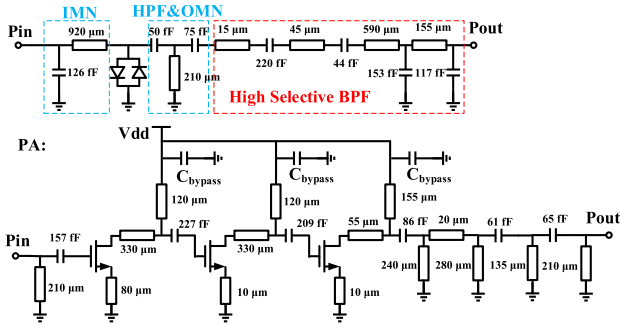


Fig. 19. Schematic of the 60-GHz frequency tripler and the following PA.

between every two blocks for the performance demonstration of each block. For instance, if we want to measure the output power of the 240-GHz multiplier chain, we use the New Wave Ezlaze II laser to cut off the output of the previous 240-GHz doubler stage and the input of the next 300-GHz mixer stage, and then, we can measure the performance of the 240-GHz multiplier chain easily. The chip is on-wafer measured with wires bonded to dc pads for dc supply.

#### A. Measurement of the 240-GHz AMC

For the 240-GHz multiplier chain test, the measurement setup is shown in Fig. 17. The input power was generated by an Agilent E8257D signal generator and a W-band OML S15MS-AG multiplier by a six-source module. Due to the lack of wideband probes and waveguides that cover the frequency band from 200 to 300 GHz, the output power was measured by the Erickson PM4 power meter in the frequency band 140–220 and 220–325 GHz, respectively. In the output path, the loss of WR03 (WR05) Infinity probe and tapers can be obtained from the datasheet, and the loss of WR03 (WR05) the S-bend waveguide is measured by the Keysight vector network analyzer with extenders. The deembedded output power versus input frequency is shown in Fig. 18. The multiplier chain achieves a measured peak output power of 5.5 dBm at 252 GHz with a 3-dB bandwidth of 48 GHz from 212 to 260 GHz. Compared with other state of the

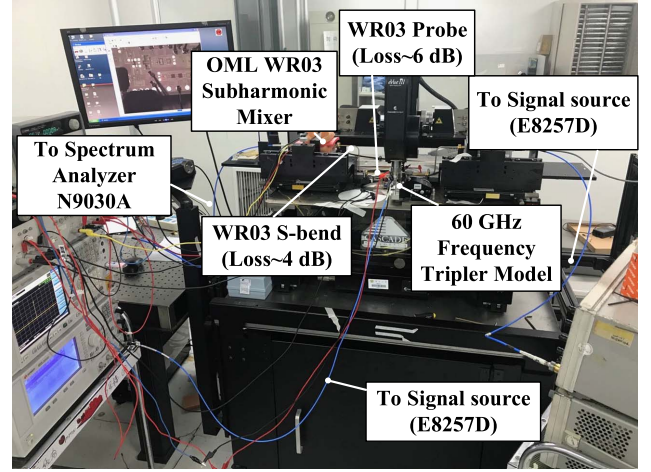


Fig. 20. Measurement setup of the proposed transmitter.

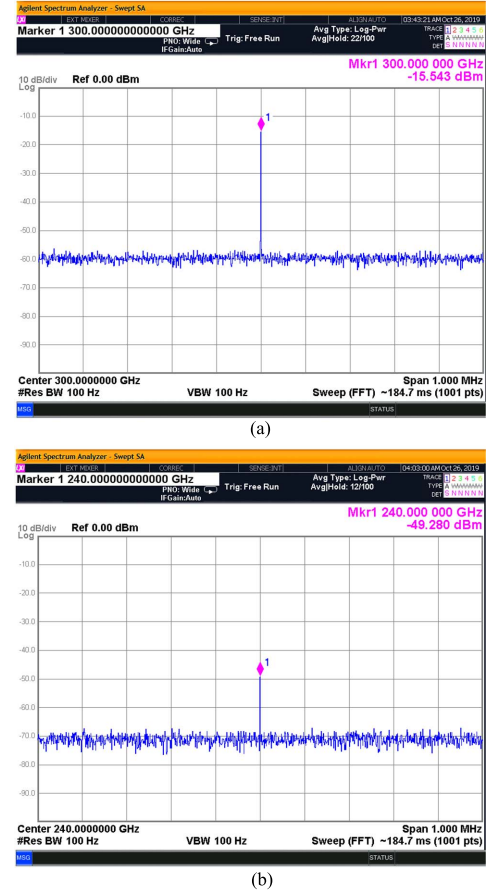


Fig. 21. Measured spectrum of (a) RF power in 1-dB compression point for  $f_{IF} = 60$  GHz,  $f_{LO} = 240$  GHz, and  $P_{IF,TX} = 3$  dBm. (b) LO leakage for  $f_{LO} = 240$  GHz.

arts shown in Table I, the proposed AMC demonstrates good output power and operating bandwidth performance.

#### B. 60-GHz Frequency Tripler for Measurement Setup

This integrated 300-GHz transmitter's input IF signal is 60 GHz. A 60-GHz tripler chip based on GaAs technology was added as an IF signal generator, as shown



TABLE I  
COMPARISON OF WITH STATE-OF-THE-ART AMC AROUND 300 GHz

Freq. (GHz)	Tech	Topology	$P_{\text{sat}}$ (dBm)	3-dB BW (GHz)	Relative BW (%)	DC-to-RF Efficiency (%)	Area (mm <sup>2</sup> )	Ref.
300	130-nm SiGe	$\times 4$ Multi. + PA + Doub	2.3	223-350	44.3	0.3	1	[22]
204	130-nm SiGe	2-way PA + Doub	6.5	170-220	25.6	1.13	NA	[23]
284	130-nm SiGe	Doub + PA + Doub	2.5	280-314	11.4	0.46	0.652	[24]
215	90-nm SiGe	4-way Comb. PA + Doub	8	200-230	14	0.23	3.63	[25]
280	130-nm SiGe	$\times 27$ Multi.	8.5*	272-288	5.7	0.72	2.8	[26]
<b>252</b>	<b>130-nm SiGe</b>	<b>Doub + PA + 2-way Doub</b>	<b>5.5</b>	<b>212-260</b>	<b>20.3</b>	<b>1.4</b>	<b>0.29</b>	<b>This work</b>

\*Radiated Power

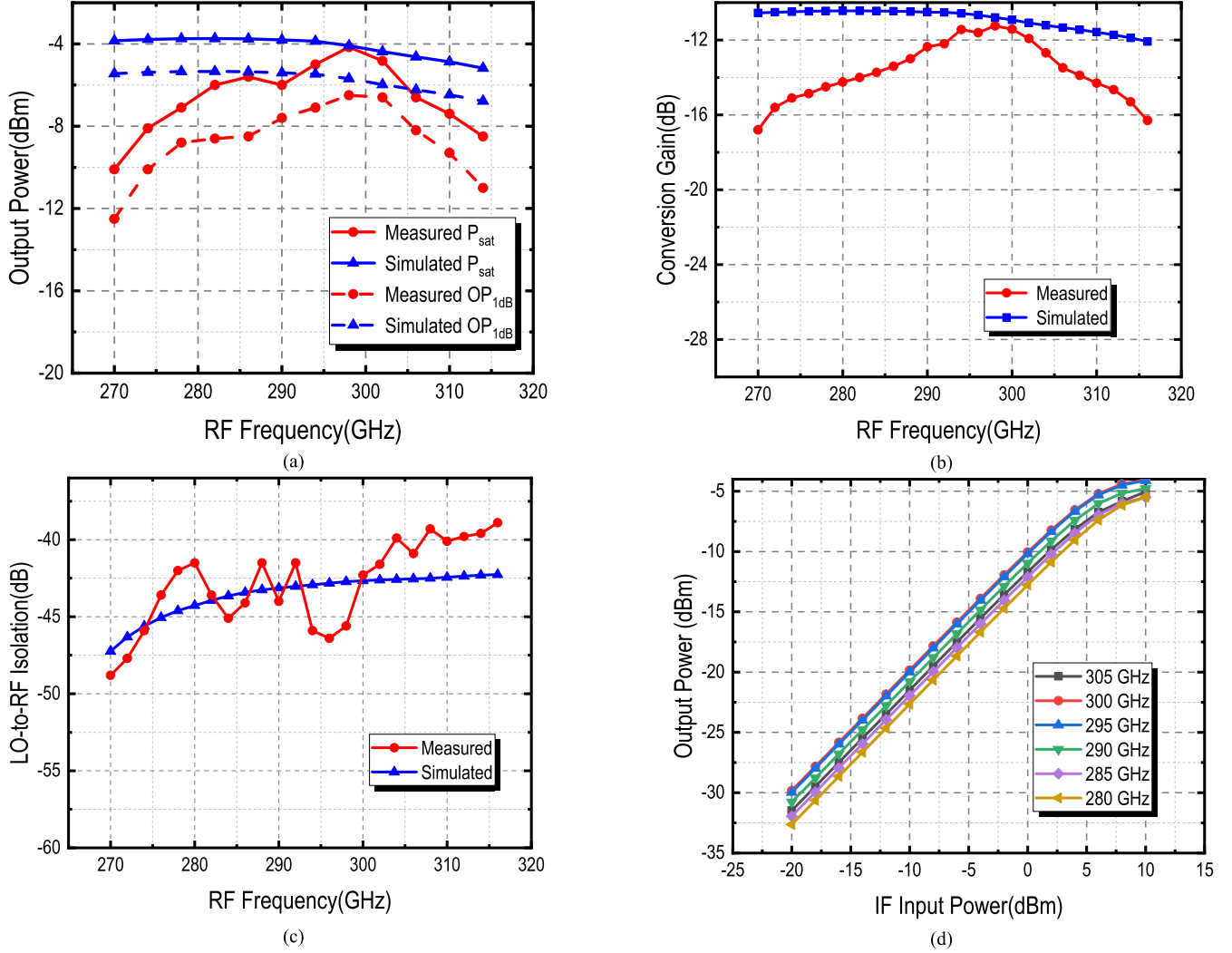


Fig. 22. Transmitter characterization results. (a) Measured and simulated saturated output power/ $OP_{1\text{dB}}$ . (b) Conversion gain at LO frequency of 240 GHz. (c) Measured and simulated LO-to-RF isolation of the transmitter. (d) Measured RF power as a function of IF input power.

in Fig. 19. This tripler model is comprised of a tripler and a three-stage common-source PA similar to our previous work [36]. The tripler consists of an antiparallel diode pair and a bandpass filter (BPF). A fifth-order high pass filter (HPF) is employed after the amplifier for fundamental and second-harmonic rejection. The saturated output power of the tripler model varies from 17 to 18.8 dBm and is sufficient for test requirements.

Considering the waveguide probe for the measurement, the tripler is integrated into a WR-12 waveguide packaging. The transition includes the RF GSG-pad-to-microstrip-line bonding wire and microstrip-line-to-waveguide transition. The insertion loss of the transition varies from  $-0.3$  to  $-0.8$  dB. In this way, the IF input frequency of the whole system is around 20 GHz and can be supplied by an Agilent E8257D signal generator.

TABLE II  
COMPARISON OF MONOLITHICALLY INTEGRATED SUB-THz TRANSMITTERS

Reference	[12]	[18]	[19]	[37]	[38]	[39]	[40]	This work
Process	0.25 $\mu\text{m}$ InP DHBt	130 nm SiGe	130 nm SiGe	40 nm CMOS	40 nm CMOS	28nm CMOS	40nm CMOS	130 nm SiGe
$f_{\text{THz}}/f_{\text{max}}$ (GHz)	370/650	300/500	300/500	<300	NA	NA	-/280	300/500
3 dB BW (GHz)	297.6-318.1	230-250	220-255	255-275 <sup>(2)</sup>	289-311	390(16)	275-305	280-310
Conversion Gain (dB)	25	16	10.5	-2 <sup>(2)</sup>	-8 <sup>(2)</sup>	NA	-10 <sup>(2)</sup>	-11.2
$P_{\text{sat}}/OP_{1\text{dB}}$ (dBm)	-2.3/-5	-6/-10	-0.8/-1.5 <sup>(1)</sup>	-1.6/-3 <sup>(2)</sup>	-5.5/-	-16/-	-14.5/-	-4.1/-6.5
$f_{\text{LO}}/P_{\text{LO}}$ (GHz/dBm)	298.1/-1.8	240/0	240/0	133/NA	145/5.5	115/-	97/-	240/5
$P_{\text{DC}}$ (mW)	452	1033	375	890	1400	1100	1400	300
Chip size ( $\text{mm}^2$ )	1.32	1.695	1.25	11.07	5.2	2	6	0.65
LO Arch	Fund Oscillator	Frequency multiplier ( $\times 16$ )	Frequency multiplier ( $\times 8$ )	Frequency multiplier ( $\times 3$ )	Frequency multiplier ( $\times 3$ )	External	External	Frequency multiplier ( $\times 4$ )
Architecture	Fund Mixer Amplifier	Fund Mixer Amplifier	Amplifier, Mixer, LO	Square Mixer	Square Mixer	Fund Mixer Tripler	Cubic Mixer	Fund Mixer

(1) Compensated for output pad

(2) Estimated from the figures.

### C. Measurement of the 300-GHz Transmitter

For the measurement of the 300-GHz transmitter, the LO power is supplied by the 240-GHz multiplier chain. The OML WR03 harmonic mixer followed by the Keysight spectrum analyzer N9030A is used for the output frequency and LO signal leakage detecting, as shown in Fig. 20. The image frequency signal and other spurious signals are difficult to be filtered, so the output power of the transmitter is measured by the spectrum analyzer, and the insertion loss of the OML WR03 subharmonic mixer is calibrated using the OML calibration table. The transmitter characterization, including conversion gain and saturated output power  $OP_{1\text{dB}}$ , and the LO-to-RF isolation are summarized in Figs. 21 and 22. Fig. 21 shows the measured output spectrum at 300 GHz and the measured LO leakage spectrum at 240 GHz with a 60-GHz IF signal. Fig. 22(a) shows the measured  $P_{\text{sat}}$  and  $OP_{1\text{dB}}$  of the transmitter front end when the IF frequency is swept and the LO frequency is fixed at 240 GHz. Fig. 22(b) shows the conversion gain of the transmitter as a function of the RF frequency swept from 275 to 315 GHz with a fixed LO frequency of 240 GHz. Fig. 22(c) shows the LO-to-RF isolation as a function of the RF frequency swept from 275 to 315 GHz with a fixed IF frequency of 60 GHz. Fig. 22(d) shows  $P_{\text{RF}}$  as a function of  $P_{\text{IF}}$ .

Across the 30-GHz 3-dB bandwidth from 280 to 310 GHz, the transmitter achieves a maximum conversion gain of  $-11.2$  dB at 298 GHz and over  $-40$ -dB LO-to-RF isolation. The transmitter consumes 300 mW in total with 3.3-V supply, where the multiplier chain consumes 270 mW, and the upconversion mixer consumes only 30 mW.

## VII. CONCLUSION

A 300-GHz monolithic integrated transmitter chipset has been demonstrated in a commercial 130-nm SiGe HBT technology. This 300-GHz transmitter consists of a 240-GHz AMC

and a 300-GHz upconversion mixer. In the sub-THz band, the most critical issues are the limited transistor performance, in terms of gain and output power. In this article, the LO AMC achieves a saturated output power of 5.5 dBm, which is sufficient to drive a 300-GHz modified Gilbert mixer. High-performance balun is also a key component in the sub-THz circuit. In this work, an SSMB with coupling coefficient enhancement is proposed, which achieves the lowest insertion loss with a compact layout at around 300 GHz, to the author's best knowledge. Over the 280–310-GHz bandwidth, the output power of the transmitter is higher than  $-7$  dBm with the maximum output power of  $-4.1$  dBm at 300 GHz. Furthermore, this transmitter exhibits a conversion gain of  $-11.2$  dB with  $OP_{1\text{dB}}$  of  $-6.5$  dBm. Compared with other state of the arts shown in Table II, the transmitter exhibits a comparable performance among silicon-based transmitters near 300 GHz with limited dc power consumption. The implemented transmitter can be used in sliding-IF or other heterodyne architecture, where IF signals [V-band (60 GHz)] are moved to the 300-GHz band for future communication systems. Besides, the presented chipset can be adapted to a number of sub-THz band imaging, radar, and sensing applications.

## ACKNOWLEDGMENT

The authors would like to thank Chen Wang, J. Ma, and T. Zhang for the chip test assistance. They would also like to thank Yuxiang Lu for revising the grammar and spelling of the article.

## REFERENCES

- [1] *IEEE Standard for High Data Rate Wireless Multi-Media Networks—Amendment 2: 100 Gb/s Wireless Switched Point-to-Point Physical Layer*, IEEE Standard 802.15.3d-2017, 2017.
- [2] H. Rucker, B. Heinemann, and A. Fox, "Half-terahertz SiGe BiCMOS technology," in *Proc. IEEE 12th Topical Meeting Silicon Monolithic Integr. Circuits RF Syst.*, Jan. 2012, pp. 133–136.

- [3] J. J. Pekarik *et al.*, "A 90 nm SiGe BiCMOS technology for mm-wave and high-performance analog applications," in *Proc. IEEE Bipolar/BiCMOS Circuits Technol. Meeting*, Sep. 2014, pp. 3.9.1–3.9.3.
- [4] P. Chevalier *et al.*, "A 55 nm triple gate oxide 9 metal layers SiGe BiCMOS technology featuring 320 GHz  $f_T$ /370 GHz  $f_{MAX}$  HBT and high-Q millimeter-wave passives," in *IEDM Tech. Dig.*, Dec. 2014, pp. 3.9.1–3.9.3.
- [5] S. Shopov, A. Balteanu, J. Hasch, P. Chevalier, A. Cathelin, and S. P. Voinigescu, "A 234–261-GHz 55-nm SiGe BiCMOS signal source with 5.4–7.2 dBm output power, 1.3% DC-to-RF efficiency, and 1-GHz divided-down output," *IEEE J. Solid-State Circuits*, vol. 51, no. 9, pp. 2054–2065, Sep. 2016.
- [6] S. Moghadami, F. Hajilou, P. Agrawal, and S. Ardalan, "A 210 GHz fully-integrated OOK transceiver for short-range wireless chip-to-chip communication in 40 nm CMOS technology," *IEEE Trans. THz Sci. Technol.*, vol. 5, no. 5, pp. 737–741, Sep. 2015.
- [7] S. Moghadami, J. Isaac, and S. Ardalan, "A 0.2–0.3 THz CMOS amplifier with tunable neutralization technique," *IEEE Trans. THz Sci. Technol.*, vol. 5, no. 6, pp. 1088–1093, Nov. 2015.
- [8] H. Bameri and O. Momeni, "A high-gain mm-wave amplifier design: An analytical approach to power gain boosting," *IEEE J. Solid-State Circuits*, vol. 52, no. 2, pp. 357–370, Feb. 2017.
- [9] D. Park *et al.*, "A 230–260-GHz wideband and high-gain amplifier in 65-nm CMOS based on dual-peak  $G_{max}$ -core," *IEEE J. Solid-State Circuits*, vol. 54, no. 6, pp. 1613–1623, Sep. 2019.
- [10] K. Tokgoz *et al.*, "A 273–301-GHz amplifier with 21-dB peak gain in 65-nm standard bulk CMOS," *IEEE Microw. Wireless Compon. Lett.*, vol. 29, no. 5, pp. 342–344, Apr. 2019.
- [11] M. H. Eissa and D. Kissinger, "4.5 A 13.5 dBm fully integrated 200-to-255 GHz power amplifier with a 4-way power combiner in SiGe:C BiCMOS," in *IEEE Int. Solid-State Circuits Conf. (ISSCC) Dig. Tech. Papers*, San Francisco, CA, USA, Feb. 2019, pp. 82–84.
- [12] S. Kim *et al.*, "300 GHz integrated heterodyne receiver and transmitter with on-chip fundamental local oscillator and mixers," *IEEE Trans. THz Sci. Technol.*, vol. 5, no. 1, pp. 92–101, Jan. 2015.
- [13] H. Hamada *et al.*, "300-GHz, 100-Gb/s InP-HEMT wireless transceiver using a 300-GHz fundamental mixer," in *IEEE MTT-S Int. Microw. Symp. Dig.*, Jun. 2018, pp. 1480–1483.
- [14] D. del Rio *et al.*, "A wideband and high-linearity E-B and transmitter integrated in a 55-nm SiGe technology for backhaul point-to-point 10-Gb/s links," *IEEE Trans. Microw. Theory Techn.*, vol. 65, no. 8, pp. 2990–3001, Aug. 2017.
- [15] C. J. Lee *et al.*, "A 120 GHz I/Q transmitter front-end in a 40 nm CMOS for wireless chip to chip communication," in *Proc. IEEE Radio Freq. Integr. Circuits Symp. (RFIC)*, Jun. 2018, pp. 192–195.
- [16] E. Öjefors, F. Pourchon, P. Chevalier, and U. R. Pfeiffer, "A 160-GHz low-noise downconverter in a SiGe HBT technology," in *Proc. 40th Eur. Microw. Conf.*, Sep. 2010, pp. 521–524.
- [17] U. R. Pfeiffer, E. Öjefors, and Y. Zhao, "A SiGe quadrature transmitter and receiver chipset for emerging high-frequency applications at 160 GHz," in *IEEE Int. Solid-State Circuits Conf. (ISSCC) Dig. Tech. Papers*, Feb. 2010, pp. 416–417.
- [18] N. Sarmah *et al.*, "A fully integrated 240-GHz direct-conversion quadrature transmitter and receiver chipset in SiGe technology," *IEEE Trans. Microw. Theory Techn.*, vol. 64, no. 2, pp. 562–574, Feb. 2016.
- [19] M. H. Eissa *et al.*, "Wideband 240-GHz transmitter and receiver in BiCMOS technology with 25-Gbit/s data rate," *IEEE J. Solid-State Circuits*, vol. 53, no. 9, pp. 2532–2542, Sep. 2018.
- [20] P. Rodríguez-Vázquez, J. Grzyb, B. Heinemann, and U. R. Pfeiffer, "A 16-QAM 100-Gb/s 1-M wireless link with an EVM of 17% at 230 GHz in a SiGe technology," *IEEE Microw. Wireless Compon. Lett.*, vol. 29, no. 4, pp. 297–299, Apr. 2019.
- [21] P. Rodríguez-Vázquez, J. Grzyb, B. Heinemann, and U. R. Pfeiffer, "A QPSK 110-Gb/s polarization-diversity MIMO wireless link with a 220–255 GHz tunable LO in a SiGe HBT technology," *IEEE Trans. Microw. Theory Techn.*, vol. 68, no. 9, pp. 3834–3851, Sep. 2020.
- [22] A. Ali *et al.*, "220–360-GHz broadband frequency multiplier chains (x8) in 130-nm BiCMOS technology," *IEEE Trans. Microw. Theory Techn.*, vol. 68, no. 7, pp. 2701–2714, Jul. 2020.
- [23] K. Wu, S. Muralidharan, and M. M. Hella, "A wideband SiGe BiCMOS frequency doubler with 6.5-dBm peak output power for millimeter-wave signal sources," *IEEE Trans. Microw. Theory Techn.*, vol. 66, no. 1, pp. 187–200, Jan. 2018.
- [24] P. Zhou, J. Chen, P. Yan, Z. Chen, D. Hou, and W. Hong, "A 280–325 GHz frequency multiplier chain with 2.5 dBm peak output power," in *Proc. IEEE Custom Integr. Circuits Conf. (CICC)*, Apr. 2019, pp. 1–4.
- [25] H.-C. Lin and G. M. Rebeiz, "A SiGe multiplier array with output power of 5–8 dBm at 200–230 GHz," *IEEE Trans. Microw. Theory Techn.*, vol. 64, no. 7, pp. 2050–2058, Jul. 2016.
- [26] N. Buadana *et al.*, "A 280-GHz digitally controlled four port chip-scale dielectric resonator antenna transmitter with DiCAD true time delay," *IEEE Solid-State Circuits Lett.*, vol. 3, no. 7, pp. 2050–2058, Jul. 2016.
- [27] E. Öjefors, B. Heinemann, and U. R. Pfeiffer, "Subharmonic 220- and 320-GHz SiGe HBT receiver front-ends," *IEEE Trans. Microw. Theory Techn.*, vol. 60, no. 5, pp. 1397–1404, May 2012.
- [28] Y. Zhao, E. Öjefors, K. Aufinger, T. F. Meister, and U. R. Pfeiffer, "A 160-GHz subharmonic transmitter and receiver chipset in an SiGe HBT technology," *IEEE Trans. Microw. Theory Techn.*, vol. 60, no. 10, pp. 3286–3299, Oct. 2012.
- [29] K. S. Ang and I. D. Robertson, "Analysis and design of impedance-transforming planar Marchand baluns," *IEEE Trans. Microw. Theory Techn.*, vol. 49, no. 2, pp. 402–406, Feb. 2001.
- [30] F. Ahmed, M. Furqan, and A. Stelzer, "A 200–325-GHz wideband, low-loss modified Marchand balun in SiGe BiCMOS technology," in *Proc. Eur. Microw. Conf. (EuMC)*, Sep. 2015, pp. 40–43.
- [31] S. Malz, P. Hillger, B. Heinemann, and U. R. Pfeiffer, "A 275 GHz amplifier in 0A3  $\mu$ m SiGe," in *Proc. 11th Eur. Microw. Integr. Circuits Conf. (EuMIC)*, Oct. 2016, pp. 185–188.
- [32] L. Xu, H. Sjöland, M. Tormanen, T. Tired, T. Pan, and X. Bai, "A miniaturized Marchand balun in CMOS with improved balance for millimeter-wave applications," *IEEE Microw. Wireless Compon. Lett.*, vol. 24, no. 1, pp. 53–55, Jan. 2014.
- [33] R. Mongia, I. Bahl, and P. Bhartia, *RF and Microwave Coupled-Line Circuits*. Norwood, MA, USA: Artech House, 1999.
- [34] P. Zhou *et al.*, "A 150-GHz transmitter with 12-dBm peak output power using 130-nm SiGe:C BiCMOS process," *IEEE Trans. Microw. Theory Techn.*, vol. 68, no. 5, pp. 342–344, Jul. 2020.
- [35] H. Li *et al.*, "A 250-GHz differential SiGe amplifier with 21.5-dB gain for sub-THz transmitters," *IEEE Trans. THz Sci. Technol.*, vol. 10, no. 6, pp. 624–633, Nov. 2020.
- [36] C. Wang *et al.*, "E-band transceiver MMIC in waveguide package for millimeter-wave radio channel emulation applications," *Sci. China Inf. Sci.*, to be published.
- [37] S. Lee *et al.*, "An 80-Gb/s 300-GHz-band single-chip CMOS transceiver," *IEEE J. Solid-State Circuits*, vol. 54, no. 12, pp. 3577–3588, Dec. 2019.
- [38] K. Takano *et al.*, "A 105 Gb/s 300 GHz CMOS transmitter," in *IEEE Int. Solid-State Circuits Conf. (ISSCC) Dig. Tech. Papers*, Feb. 2017, pp. 308–309.
- [39] A. Standaert and P. Reynaert, "A 390-GHz outphasing transmitter in 28-nm CMOS," *IEEE J. Solid-State Circuits*, vol. 55, no. 10, pp. 2703–2713, Oct. 2020.
- [40] K. Katayama *et al.*, "A 300 GHz CMOS transmitter with 32-QAM 17.5 Gb/s/ch capability over six channels," *IEEE J. Solid-State Circuits*, vol. 51, no. 12, pp. 3037–3048, Dec. 2016.



**Jiayang Yu** (Student Member, IEEE) is currently pursuing the Ph.D. degree in electromagnetic field and microwave technique from the School of Information Science and Engineering, State Key Laboratory of Millimeter Waves, Southeast University, Nanjing, China. His research interests include millimeter-wave integrated circuits for radar and high-speed communication.

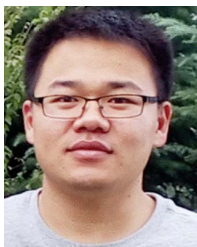




**Jixin Chen** (Member, IEEE) was born in Jiangsu, China, in 1976. He received the B.S. degree in radio engineering and the M.S. and Ph.D. degrees in electromagnetic field and microwave technique from Southeast University, Nanjing, China, in 1998, 2002, and 2006, respectively.

Since 1998, he has been with the State Key Laboratory of Millimeter Waves, Southeast University. He is currently a Professor with the School of Information Science and Engineering and the Director of the Department of Electromagnetic Field and Microwave Engineering, Southeast University. His current research interests include microwave and millimeter-wave circuit design and monolithic microwave integrated circuit (MMIC) design.

Dr. Chen was a recipient of the 2016 Keysight Early Career Professor Award and the 2016 National Natural Science Prize Second Prize. He served as the TPC Chair for RFIT2019 and the TPC Co-Chair for HSIC2012 and UCMMT2012.



**Peigen Zhou** (Member, IEEE) received the B.S. degree from the School of Information Science and Engineering, Southeast University, Nanjing, China, in 2015, where he is currently pursuing the Ph.D. degree.

Since 2019, he has been a Visiting Student Researcher with Eindhoven University of Technology, Eindhoven, The Netherlands. His current research interests include silicon-based millimeter-wave/terahertz (THz) on-chip wireless communication/radar phased-array transceivers.

Mr. Zhou was a recipient of the National Scholarship in 2016, the second prize of the National Institute of Mathematical Modeling Competition in 2016, the Rohde-Schwarz Ph.D. Scholarship in 2017, the Vanchip Ph.D. Scholarship in 2019, and the IEEE International Conference on Microwave and Millimeter Wave Technology (ICMMT) Best Student Paper Award.



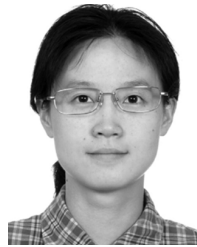
**Zekun Li** (Graduate Student Member, IEEE) was born in Fujian, China, in 1996. He received the B.S. degree from the School of Information Science and Engineering, Southeast University, Nanjing, China, in 2018, where he is currently pursuing the Ph.D. degree.

His current research is focused on silicon-based mm-wave and terahertz (THz) integrated circuits and systems for high-speed wireless communication.



**Huanbo Li** was born in Zhejiang, China, in 1993. He received the B.S. degree from the School of Information Science and Engineering, Southeast University, Nanjing, China, in 2016, where he is currently pursuing the Ph.D. degree.

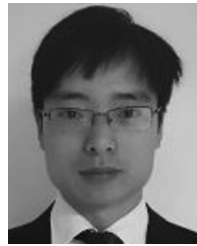
He is currently a Trainee with MISIC Microelectronics, Nanjing. His current research is focused on silicon-based mm-wave and terahertz (THz) integrated circuits and systems for high-speed wireless communication and radar imaging.



**Pinpin Yan** (Member, IEEE) received the B.S. degree in radio engineering and the M.S. and Ph.D. degrees in electromagnetic field and microwave technique from Southeast University, Nanjing, China, in 2000, 2004, and 2009, respectively.

Since 2000, she has been with the State Key Laboratory of Millimeter Waves, Southeast University, where she is currently an Associate Professor with the School of Information Science and Engineering.

Her current research interests include microwave and millimeter-wave circuit design and monolithic microwave integrated circuit (MMIC) design.



**Debin Hou** (Member, IEEE) was born in Sichuan, China, in 1983. He received the B.S. degree from the School of Physical Electronics, University of Electronic Science and Technology of China (UESTC), Chengdu, China, in 2007, and the Ph.D. degree from the School of Information Science and Technology, Southeast University, Nanjing, China, in 2013.

From 2009 to 2012, he was with Blekinge Institute of Technology (BTH), Karlskrona, Sweden, and the Institute of Microelectronics (IME), Agency for Science, Technology and Research (A\*STAR),

Singapore, as an Exchange Student. Since 2013, he has been with the State Key Laboratory of Millimeter Waves, Southeast University, where he is currently an Associate Professor with the School of Information Science and Engineering. He has authored or coauthored more than 20 technical publications. His current research interests include silicon-based/GaAs millimeter-wave/terahertz (THz) on-chip components, antennas, and integrated circuits.

Dr. Hou was a recipient of the "Jiangsu Excellent 100 Doctoral Dissertation" prize in 2014.



**Wei Hong** (Fellow, IEEE) received the B.S. degree in radio engineering from the University of Information Engineering, Zhengzhou, China, in 1982, and the M.S. and Ph.D. degrees in radio engineering from Southeast University, Nanjing, China, in 1985 and 1988, respectively.

In 1993, 1995, and 1996–1998, he was a short-term Visiting Scholar with the University of California at Berkeley, Berkeley, CA, USA, and the University of California at Santa Cruz, Santa Cruz, CA. Since 1988, he has been with the State Key

Laboratory of Millimeter Waves, Southeast University, and has been serving as the Director for the laboratory, since 2003. He is currently a Professor with the School of Information Science and Engineering, Southeast University. He has authored and coauthored more than 300 technical publications and two books. He has been engaged in numerical methods for electromagnetic problems, millimeter-wave theory and technology, antennas, RF technology for wireless communications, and so on.

Dr. Hong is a Fellow of CIE, the Vice President of the CIE Microwave Society and Antenna Society, and the Chair of the IEEE MTT-S/AP-S/EMC-S Joint Nanjing Chapter. He was an elected IEEE MTT-S AdCom Member from 2014 to 2016. He twice awarded the National Natural Prizes, thrice awarded the first-class Science and Technology Progress Prizes issued by the Ministry of Education of China and Jiangsu Province Government, and so on. Besides, he received the Foundations for China Distinguished Young Investigators and for "Innovation Group" issued by NSF of China. He served as an Associate Editor for the IEEE TRANSACTIONS ON MICROWAVE THEORY AND TECHNIQUES from 2007 to 2010.